Journal of Applied Fluid Mechanics, Vol. 15, No. 5, pp. 1333-1344, 2022.
Available online at www.jafmonline.net, ISSN 1735-3572, EISSN 1735-3645.
https://doi.org/10.47176/jafm.15.05.1015

A Passive Micromixer with Koch Snowflakes Fractal Obstacle in Microchannel

L. Hasanah [1†], D. F. Nurvadila[1], R. E. Pawinanto[2], B. Mulyanti[2], C. Wulandari[1,3], A. Aminudin[1] and J. Yunas[4]

[1] *Departement of Physics Education, Universitas Pendidikan Indonesia, Bandung, Jawa Barat, 40154, Indonesia*
[2] *Departement of Electrical Engineering Education, Universitas Pendidikan Indonesia, Bandung, Jawa Barat, 40154, Indonesia*
[3] *Engineering Physics, Institut Teknologi Bandung, Bandung, Jawa Barat, 40132, Indonesia*
[4] *Institute of Microengineering and Nanoelectronics (IMEN), Universiti Kebangsaan Malaysia (UKM), Bangi, Selangor, 43600, Malaysia*

†*Corresponding Author Email: lilikhasanah@upi.edu*

(Received December 8, 2021; accepted May 7, 2022)

ABSTRACT

The passive micromixer is one of the essential devices that can be integrated into the Lab on Chip (LoC) system. Micromixer is needed to increase mixing efficiency. In this paper, two Koch fractal obstacle-based micromixer models of Secondary Snowflakes Fractal Micromixer (SSFM) and Tertiary Snowflakes Fractal Micromixer (TSFM) were designed. The effect of the Koch fractal resistance angles (15º, 30º, 45º, 315º, 330º, 345º) and the influence of the inlet (T and T-vortex) were studied in this paper using COMSOL Multiphysics numerical simulations. The results showed that the TSFM structure with a 30º angle on the T-vortex inlet is optimal. The deflection phenomena generated by the TSFM obstacle enhance the contact area between the two fluids and chaotic convection can be increased at Reynolds Number (Re) 0.05 and Re 100. This paper examines concentration curves along the channel ranging from 1 mol/L to 5 mol/L. This clearly shows that the fluid flow direction changes within the microchannel. This work provides a new design for the micromixer.

Keywords: Micromixer; Secondary snowflakes fractal micromixer; Tertiary snowflakes fractal; Micromixer; Obstacle; Lab on chip; Microchannel; T-vortex inlet structure.

NOMENCLATURE

μ	dynamic viscosity	M	mixing efficiency
ρ	density	a	geometry width
u	velocity of fluid	b	geometry length
p	pressure	N	total number of sampling points
D	diffusion coefficient	c_i	mass fraction of sampling at point i
c	concentration	$\bar{c}$	mean of the mass fraction
Re	Reynolds number	D_h	diameter hydraulic
P	structure length	t_k	Koch fractal depth
L	structure width	l_k	Koch fractal width
t	structure height	P_k	Koch fractal length
P_i	inlet length	A	Koch fractal angle
L_i	inlet width	s	distance between fractal

1. INTRODUCTION

Lab on Chip (LoC) is a device that combines one or more laboratory functions onto a single integrated chip (Keçili *et al.* 2020). The use of this device is growing because it is widely used in various fields including microchemical analysis (Lv *et al.* 2021), chemical synthesis (Thiermann *et al.* 2017), clinical diagnosis (Fatimah *et al.* 2020), and others. The micromixer is one part of the LoC based on a mechanical micro-section that is used to mix liquid

volumes on the microliter or nanoliter scale (Chen and Zhang 2018). This represents an important topic to study because the development characteristics of the micromixer chips are multi-function (Hama *et al.* 2018), miniaturisation (Pawinanto *et al.* 2020), portable (Rohman *et al.* 2020), and small dimensions from millimetre to micrometre (Lv and Chen 2021). However, the fluid is notoriously slow to mix because of the low Reynolds number (Re) of the fluid flow in the microchannel (Borgohain *et al.* 2018). A turbulent flow has a Re number of > 2300 while a laminar flow has a Re number of < 2300 (Bayareh *et al.* 2019). Mixing in turbulent flow is a highly efficient form of chaotic convection. In contrast, laminar flow only takes advantage of the inefficient passive molecular diffusion phenomenon (Chen *et al.* 2020). Complete mixing relies on the molecular diffusion process that takes tens of centimetres or even meters (Balasubramaniam *et al.* 2017). Integrating such a long channel into a microfluidic chip is very difficult (Mehrdel *et al.* 2018). Therefore, various types of micromixer designs have been proposed to investigate the mixing process by reducing the mixing length and increasing the mixing efficiency (Mondal *et al.* 2019; Chen *et al.* 2020).

The micromixer is generally divided into two namely the active micromixer and the passive micromixer (Bayareh, 2021). Active micromixers can increase mixing efficiency by utilising external forces such as pressure (Huang *et al.* 2020), electromagnetic (Chen and Kim 2018; Bahrami *et al.* 2020), electroosmotic (Usefian and Bayareh 2019), and piezoelectric (Liu *et al.* 2018). However, equipment becomes more complex, challenging to integrate into LoC systems, and high cost (Bayareh *et al.* 2020). In contrast to active micromixers, passive micromixers do not use any external actuator to drive the fluids (Usefian and Bayareh 2019). Therefore, in this case, the passive micromixer provides more advantages than the active micromixer because it is easier to integrate into the LoC system with a low fabrication cost (Chen *et al.* 2021; Cai *et al.* 2017; Raza and Kim 2020).

Previous studies have developed many structures of lamination-based passive micromixers (Chen and Li 2017), obstacle (Zhang *et al.* 2019) convergence-divergent (Raza and Kim 2020), and asymmetrical structures (Rafeie *et al.* 2017). However, Bayerah *et al.* (2020) reported that the obstacle-based structure has the advantage of reducing the length of the channel, especially in simple designs such as the T channel. Another study by Chen and Zhao (2017) showed that obstacles can disrupt the flow of the liquids and produce turbulence to increase the mixing effectiveness. Various obstacles such as triangular obstacle (Shi *et al.* 2021), rectangular obstacle (Bazaz *et al.* 2016), curved obstacle (Borgohain *et al.* 2018), Koch fractal obstacle (Chen *et al.* 2019) have been submitted previously.

The effect of fractal-level roughness on the mixing of passive micromixers with low Re numbers has been studied (Wu and Chen 2019). The fractal theory has been applied in the field of micromixers such as fractal cantors (Shi *et al.* 2021), fractal-like trees (Chen *et al.* 2020), Koch fractal (Shi *et al.* 2021), and others. By adjusting obstacles of various shapes, the micromixer can achieve better mixing at lower Re (Sarma and Patowari 2016). Zhang *et al.* (2019) studied the fractal principle to change the barrier structure by increasing the fractal barrier effect, which is predicted to increase the mixing efficiency. In this case, the researcher simulated the primary and secondary fractal structures. The simulation results show that the secondary fractal structure has better mixing efficiency up to >60 % (Zhang *et al.* 2019). However, based on that study, the enhancement was carried out only up to the secondary fractal structure. Moreover, Ansari *et al.* (2012) studied a T-vortex inlet structure combined with other structures to improve the mixing performance.

In this paper, we investigate the principle of the Koch fractal by increasing the level of the Koch fractal combined with the T-vortex structure. The combination between Koch fractal and T-vortex is expected to improve mixing performance. Furthermore, the channel length of the micromixer can be obtained below 5.3 mm. The study was carried out in the range of Re 0.05-100 with a channel length of <8 mm. This study is expected to achieve better mixing efficiency of >0.8 in various Re.

2. GEOMETRY STRUCTURE

The micromixer was first designed using the SOLIDWORK application and then simulated using the COMSOL Multiphysics application. The fractal principle is applied in designing the resistance structure. Fig. 1 illustrates the Koch fractal concept schematically.

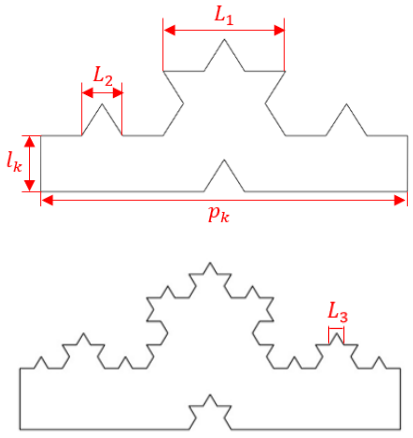

Fig. 1. Schematic diagram of Koch fractal principle.

According to the Koch fractal principle in Fig. 1, the part of the triangle formed is an equilateral triangle. The model of the micromixer with the Koch fractal resistance designed in this paper is shown in Fig. 2. Figure 2 is designed to have two inlets and one outlet with the inlet width half of the width of the main structure forming a T and T-vortex. In this case, we studied the influence structure of the Secondary

Snowflakes Fractal Micromixer (SSFM) and Tertiary Snowflakes Fractal Micromixer (TSFM). The two Koch fractal obstacle structures consist of eight pieces placed at the top of the channel wall and the bottom. The effect of the obstacle angle (A) was studied with optimal results combined on the main channel structure of the T-vortex. The design has a primary channel structure namely *P*, *L*, and *t* of $5 \times 0.30 \times 0.20$ mm, respectively. Various other parameters of the structural design used are shown in Table 1.

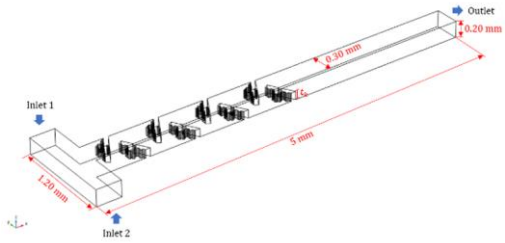

(a)

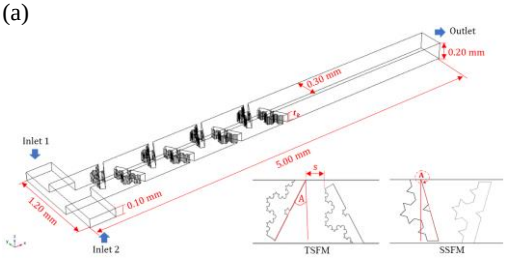

(b)

Fig. 2. Schematic diagram of micromixer models with Koch fractal obstacles, (a) inlet structure T, (b) inlet structure T-vortex.

Table 1 Parameter study based on the structures of the micromixer used

Parameter	Value
P	5 mm
L	0.30 mm
t	0.20 mm
P_i	1.20 mm
L_i	0.10 mm
P_k	2.97×10^{-1} mm
L_1	0.99×10^{-1} mm
L_2	0.33×10^{-1} mm
L_3	0.11×10^{-1} mm
l_k	0.05 mm
t_k	0.10 mm
s	0.10 mm
A	15°, 30°, 45°, 315°, 330°, & 345°

3. GOVERNING EQUATION

In this case, the fluid is considered a continuous medium under this microchannel geometry. The simulation stages that support this process used the physics module as the laminar flow (spf) and transport of diluted species (tds) configured to handle fluid mixing. Water is utilised as the fluid with a density of 1025 kg m^{-3} and the viscosity of the water is 1.5 x 10^{-3} kg m^{-1} s^{-1}. Water is assumed to have different concentrations, set C_1 is 1 mol/L and set C_2 is 5 mol/L. In addition, boundary conditions used are incompressible, Newtonian and the channel condition is no slip in the walls. Therefore, the governing equations are the equation of continuity for incompressible at Eq. (1), the Navier Stokes equation at Eq. (2), and the diffusion convection equation at Eq. (3).

$$\nabla u = 0 \tag{1}$$

$$\rho\left[\frac{\partial u}{\partial t} + (u.\nabla)u\right] = -\nabla p + \mu\nabla^2 u \tag{2}$$

$$\frac{\partial c}{\partial t} = D\nabla^2 - u.\nabla c \tag{3}$$

Where μ is dynamic viscosity, ρ is density, u is the velocity of the fluid, p is pressure, c is concentration constant, and D is the diffusion coefficient at each concentration. To better express the fluid flow, velocity parameters are needed to determine the flow velocity. This is obtained from the dimensionless parameter Re by writing it as in Eq. (4).

$$u = Re\frac{\mu}{\rho D_h} \tag{4}$$

Where u is the fluid velocity, μ is dynamic viscosity, ρ is density, and D_h is the hydraulic diameter. Eq. (6) can be used to calculate the mixing efficiency from Eq. (5) about the standard deviation.

$$\sigma = \sqrt{\frac{1}{n}\sum_{i=1}^{n}(Ci - Cs)^2} \tag{5}$$

$$M = 1 - \sqrt{\frac{\sigma^2}{\sigma_{max}^2}} \times 100\% \tag{6}$$

Where σ indicates the concentration at a certain cross-section of the mixing micromixer, n is the sampling point in the cross-section. C_i is the mass fraction of sampling at a point i, C_s is the mass fraction in question, and σ_{max} is the standard deviation at the inlet. The value of the mixing efficiency M is between 0, which means mixing (0%) or no mixing occurs, and 1 which means homogeneous mixing (100%). When the mixing range is between 0.8<M<1, it can be considered that the mixing efficiency is very high.

4. RESULT AND DISCUSSION

The mixing efficiency is affected by the mesh size used. The mesh size can be decreased by up to 20% depending on the fineness or coarseness of the mesh selected. Figure 3 depicts the local line velocity profile of the secant near the outlet at Re 1. The number of grids has been tested using the same microchannel. Based on Fig. 3, the grids number around 17180431 show the most optimal results. However, in the structure to be tested, the author use a mesh size of 2873952 due to the limited specifications of the laptop used. Considering the

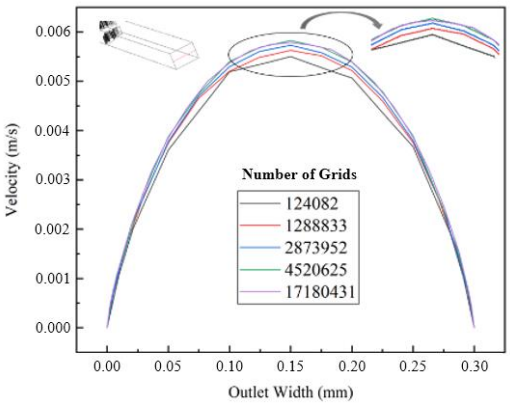

Fig. 3. Local velocity profiles of cutting line in the Outlet at Re =1 for various number of grids.

light blue curve, it remains near to the pink curve indicating that the 2873952 grid number remains completely accurate and effective in solving the structure of the Koch fractal micromixer.

The effect of angle with the main channel T was investigated for its performance on SSFM and TSFM geometric structures. Figure 4 shows the mixing performance on the SSFM structure with angles of 15º, 30º, 45º, 315º, 330º, and 345º. Figure 3 shows the mixing efficiency with respect to the angle changes in the SSFM geometric structure with a fractal obstacle depth of 0.10 mm. At Re 0.1 to 1, mixing efficiency decreased and then increased again at Re 10 and 100. However, at Re 10 angle 345º and 330º, there is a difference in which the results of the mixing efficiency decrease and then increase at Re 100. This may be caused by the convergent flow flowing at that angle having more complicated resistance than angle 315º. Therefore, the flow with a certain flow velocity result in lower mixing efficiency. However, in the six corner configurations, mixing efficiency results are >0.84 with the best average results at an angle of 30°.

Figure 5 depicts the impact of the obstacle angle on the TSFM geometric structure's mixing efficiency. Mixing efficiency decreased between Re 0.1 and 1 before increasing between Re 10 and 100. The six angle configurations get mixing efficiency results >0.84 with the best average results at an angle of 30°. From the two structures, the optimum average mixing efficiency at an angle of 30° is obtained. Figure 5 shows various angles comparison of TSFM structure.

Figure 6 compares the mixing efficiency of the SSFM and TSFM structures. Both formed the same pattern with the mixing efficiency with the TSFM micromixer pattern is better than SSFM at an angle of 30°. In particular, the mixing efficiency reaches approximately >0.91 at Re 0.05 and 100. The TSFM structure has the best results because the structure is coarser than the SSFM structure. The elements that influence the mixing efficiency of the TSFM structure are also investigated in this study.

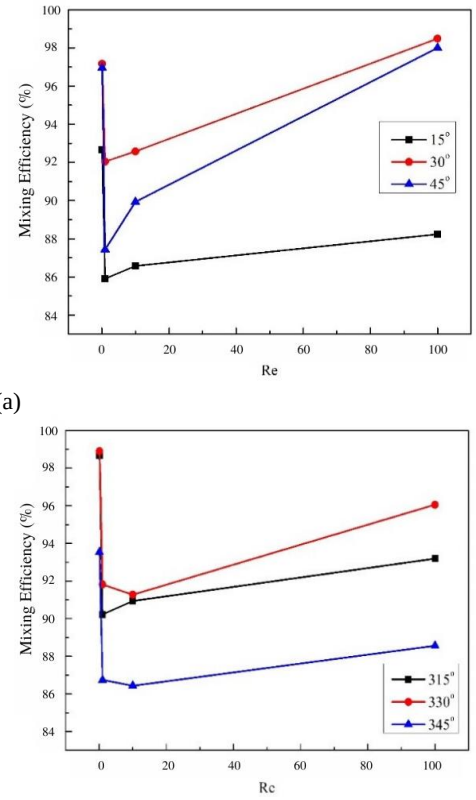

(a)

(b)

Fig. 4. Effect of angle on the mixing efficiency of the SSFM structure, (a) angle of 15º, 30º, and 45º, (b) angles of 315º, 330º, and 345º.

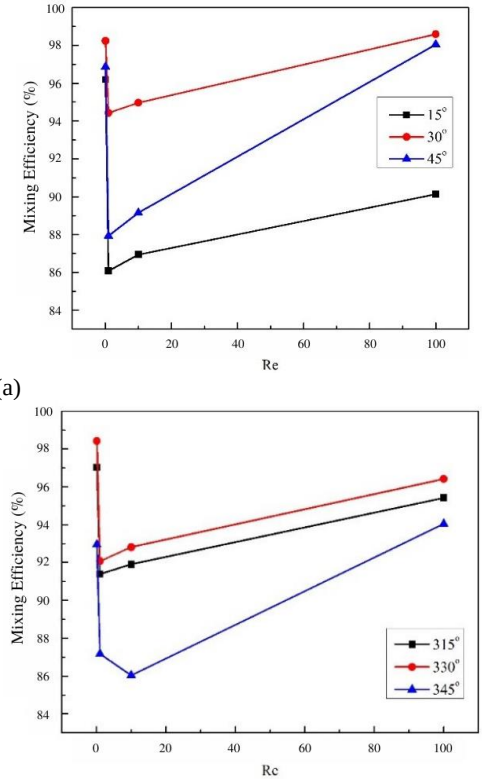

(a)

(b)

Fig. 5. Effect of angle on the mixing efficiency of the TSFM structure, (a) angle of 15º, 30º, and 45º, (b) angles of 315º, 330º, and 345º.

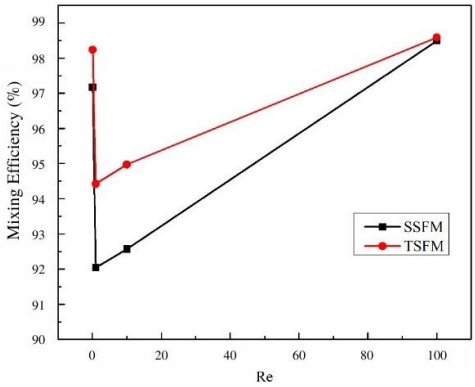

Fig. 6. Comparison of SSFM and TSFM geometric structures at angles of 30º, with Re 0.1, 1, 10, and 100.

Figure 7 shows the mixing efficiency of the TSFM obstacle structure with an angle of 30° at Re 0.05-100. The micromixer's mixing efficiency yields a result pattern similar to that seen in Fig. 5. Re 0.05, 0.1, 50, and 100 obtained mixing efficiency of >0.98, which is nearly perfect. At Re 0.05-5, mixing efficiency decreased. This occurs due to the factor of chaotic convection at high Re and molecular diffusion at low Re. In addition, to prove the influence of the T-vortex main channel structure, we combined the T-vortex inlet channel with the TSFM structure. After that, the results were compared with the results in the T channel structure as shown in Fig. 8.

Figure 8 shows that the T-vortex main channel structure can help improve the mixing efficiency compared to the T channel structure in all Re. T-vortex can improve the mixing fluid at the inlet junction before entering the applied obstacle area. Due to the mixing efficiency of >0.84, it is an indication that the fluid in the two structures has been mixed homogeneously. To prove this, Fig. 9 shows the concentration distribution on the TSFM channel structure.

The simulation of the micromixer's concentration at Re 0.05, 5, and 100 are shown in Fig. 9 and the colour legend indicates the change in the concentration from 1 mol/L and 5 mol/L to 3 mol/L, showing homogenous mixing. Liquids of different concentrations are distributed symmetrically when flowed into the microchannel. The contact occurs when the liquid goes to the junction between the liquids of different concentrations and mixing is increased as the liquid enters the mixing area formed by the TSFM obstacle structure. The liquid deflects in the microchannels significantly and the changes in the concentration are distributed symmetrically up and down on both sides of the mixing region. It increases the contact between the fluids in the microchannel and the diffusion efficiency of the molecules.

The high fluid concentration is not distributed upwards at Re 0.05 and vice versa. This phenomenon occurs due to the relatively low deflection effect on the fluid. Low Re means low flow velocity causes the fluid to be almost wholly mixed at the outlet. While

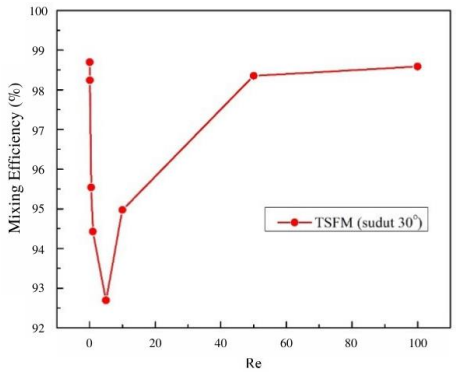

Fig. 7. Mixing efficiency of the TSFM obstacle structure with angle 30° at Re (0.05, 0.10, 0.50, 1, 5, 10, 50, and 100).

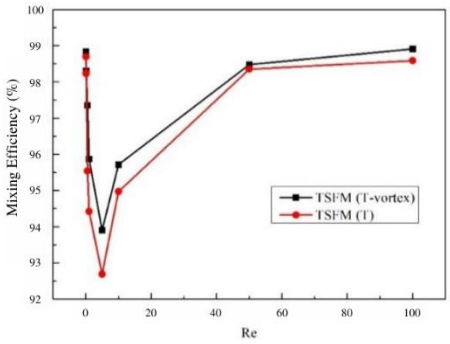

Fig. 8. Mixing efficiency results at the inlet T and T-vortex.

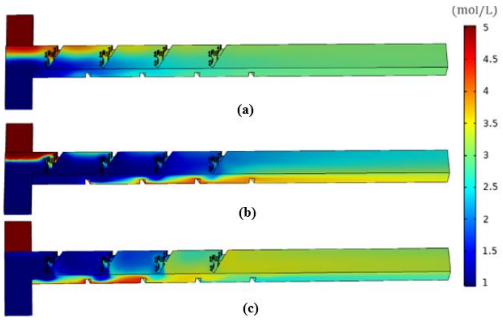

Fig. 9. Concentration distribution of the TSFM obstacle structure (a) Re 0.05, (b) 5, and (c) 100, with T-vortex inlet structure, and angle 30º.

at Re 5 and 100, the fluid flow velocity increases, the chaotic convection event is more significant, and the fluid deflection in the area is significant. Furthermore, chaotic convection event and fluid deflection produced by obstacles can increase mixing performance significantly at Re 100. To strengthen the fluid flow analysis in the microchannels and to investigate the influence of fluid deflection on the mixing efficiency, nine sample concentration parts in microchannels were selected and are illustrated in Fig. 10.

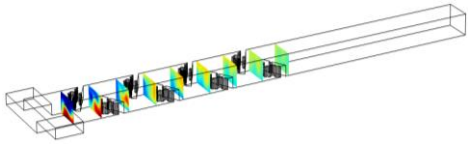

Fig. 10. Nine parts of representative concentration.

Figure 10 shows nine representative concentrations that can be used to investigate the concentration allocation and the phenomenon of fluid deflection in each section when liquid flows in the microchannel. Figures 11-13 show the direction of the fluid flow when flowing at Re 0.05, 10, and 100. The arrows indicate the direction of the fluid flow in each section, and the arrow colours indicate concentration distribution.

Figure 11 shows the fluid deflection in a fluid flowwith Re 0.05. When entering the mixing area of

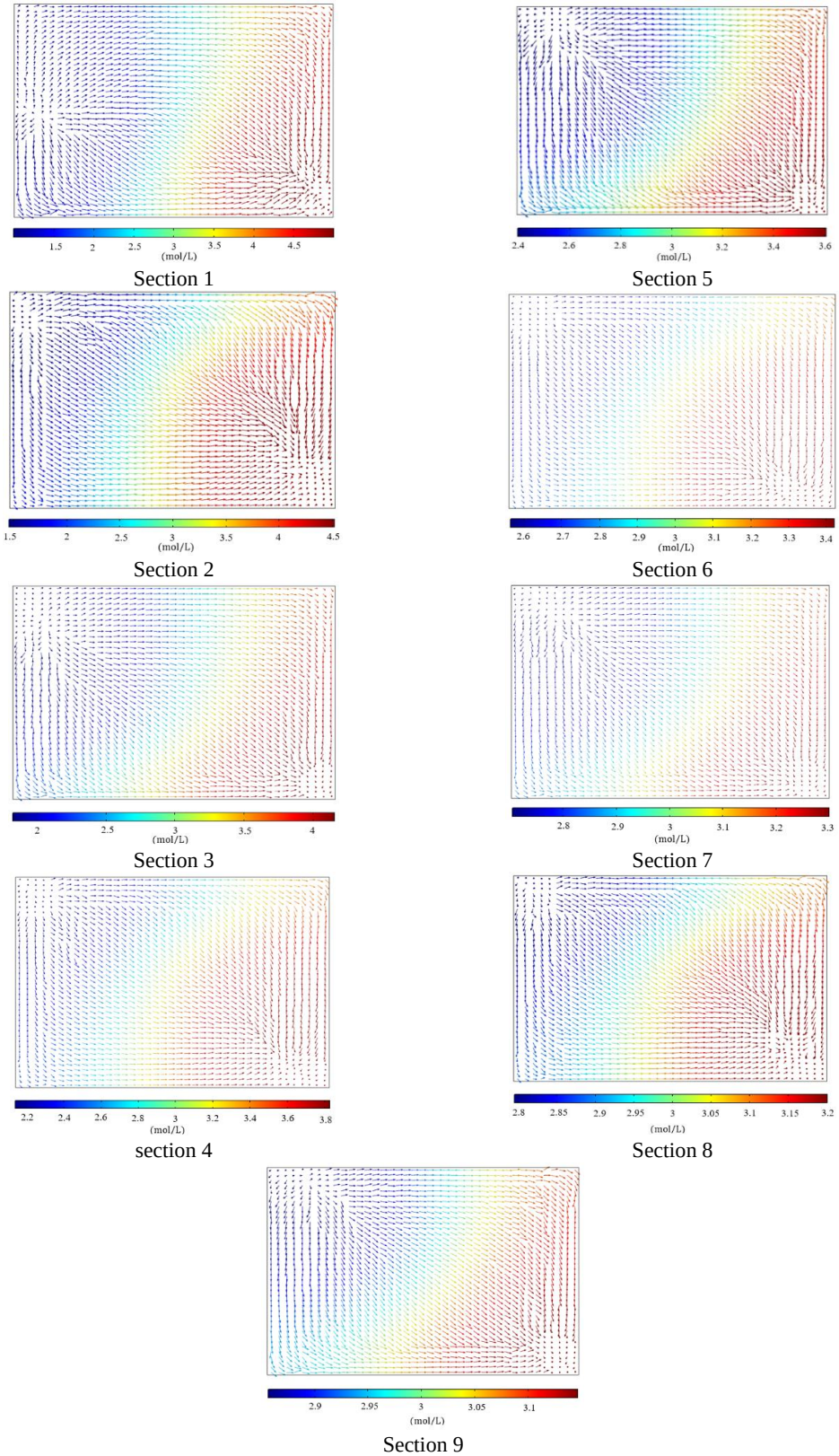

Fig. 11. Velocity field and concentration distribution field of TSFM at Re 0.05.

the obstacle structure, liquids having different concentrations are distributed symmetrically. The deflection tends to become more noticeable when the liquid enters sections 5-9, thus providing a greater contact area. It plays an essential role in increasing the mixing efficiency.

Figure 12 shows the fluid deflection in a flow with Re 5 resulting in a chaotic convection phenomenon, which is relatively better than at Re 0.05. However, due to the effect of short residence time in the microchannels, complete mixing could not be attained in section 9.

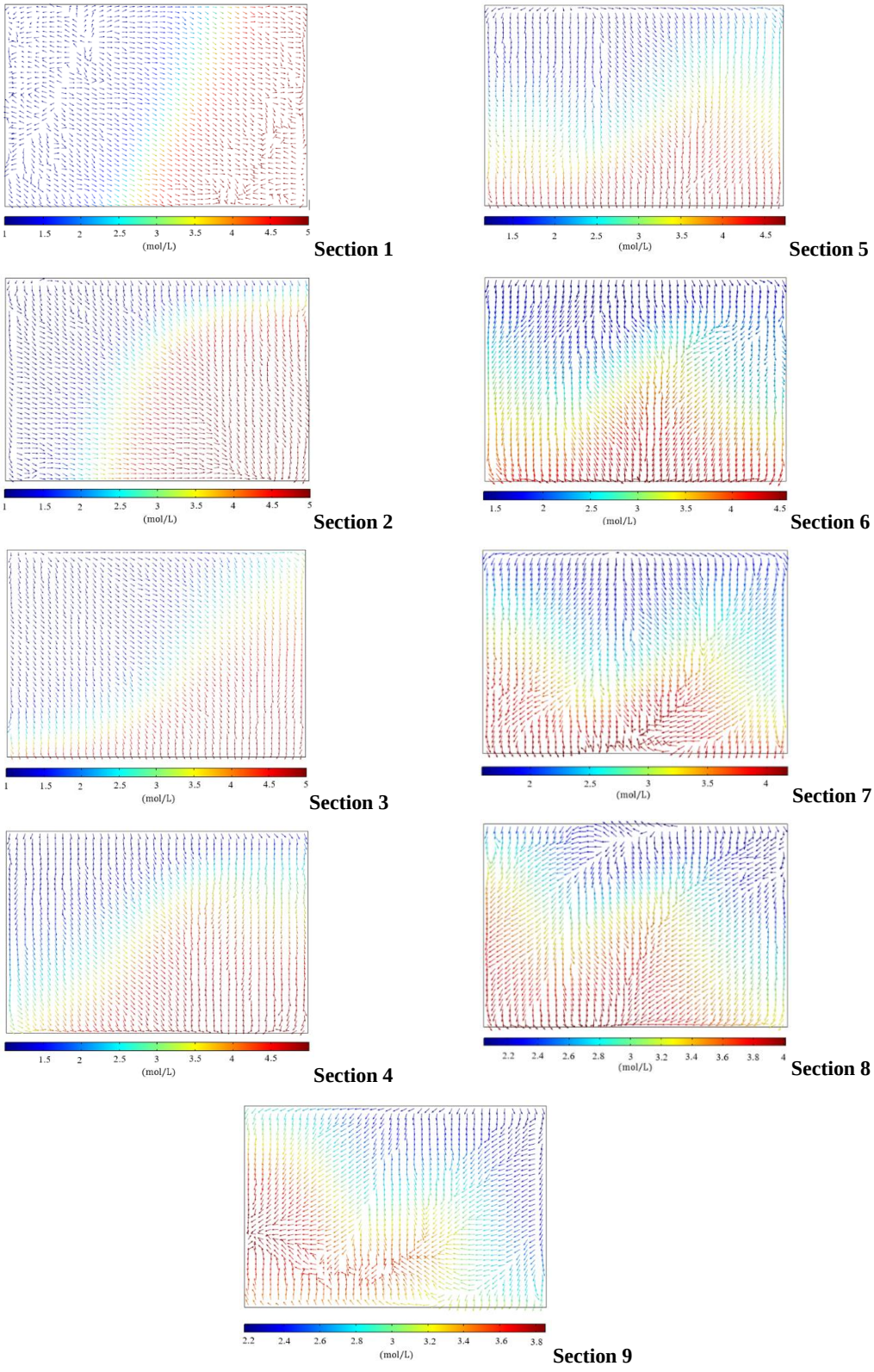

Fig. 12. Velocity field and concentration distribution field of TSFM at Re 5.

Figure 13 shows the fluid deflection in a flow with Re 100. At Re 100, it has the highest velocity compared to the others. There is a vortex that can help increase the chaotic convection of the liquid because there is a significant change in sections 4-9.

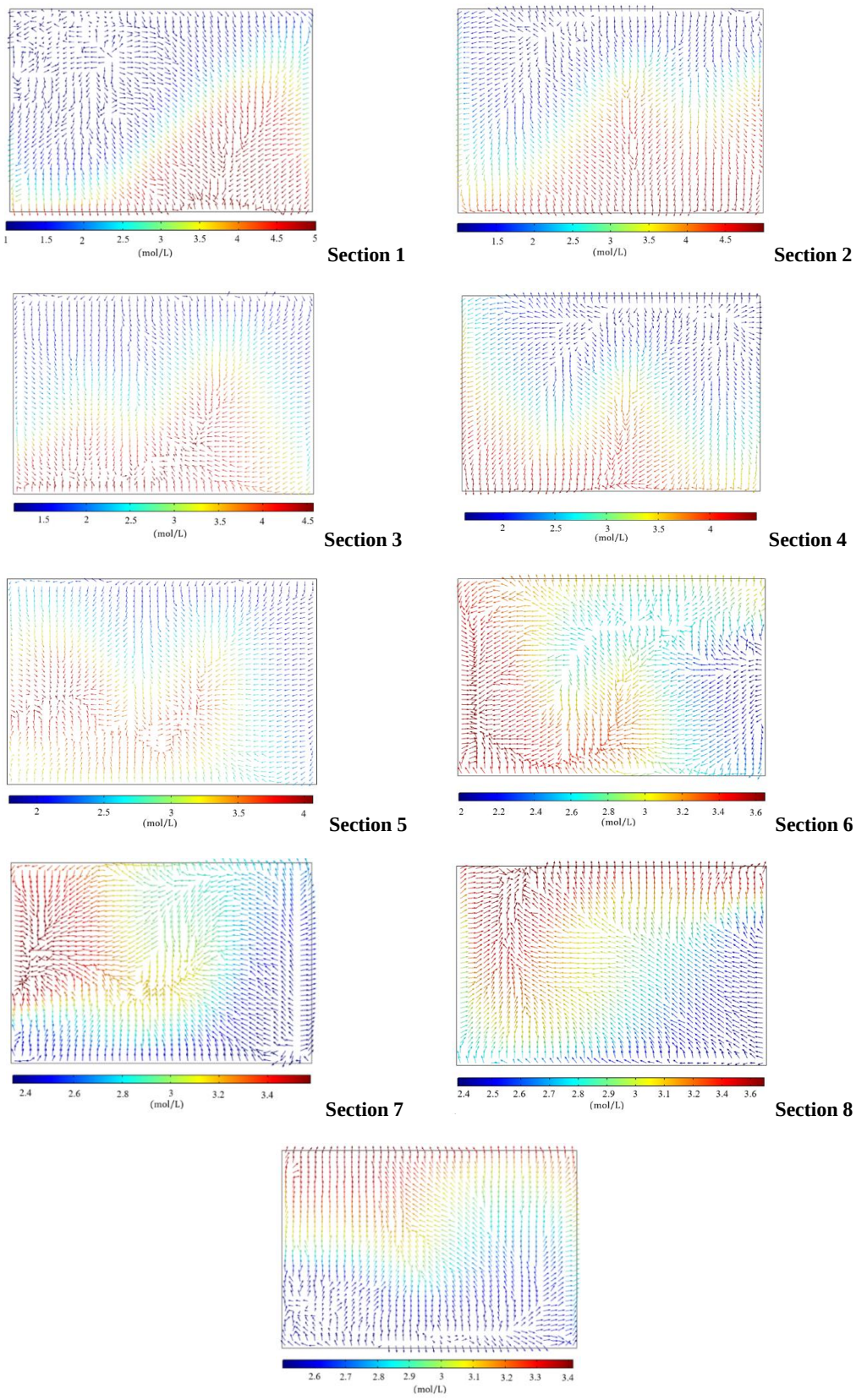

Fig. 13. Velocity field and concentration distribution field of TSFM at Re Re 100.

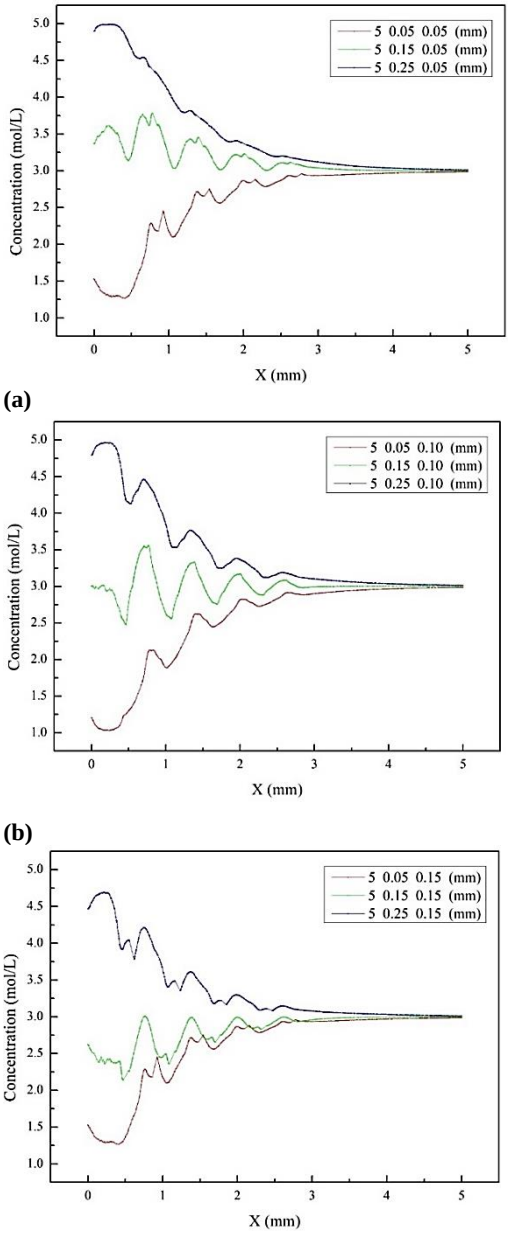

Fig. 14. Micromixer concentration curve along the X-axis direction with locations represented (y = 0.05, 0.15, 0.25 and a) z 0.05, b) z 0.10, c) z 0.15) at Re 0.05.

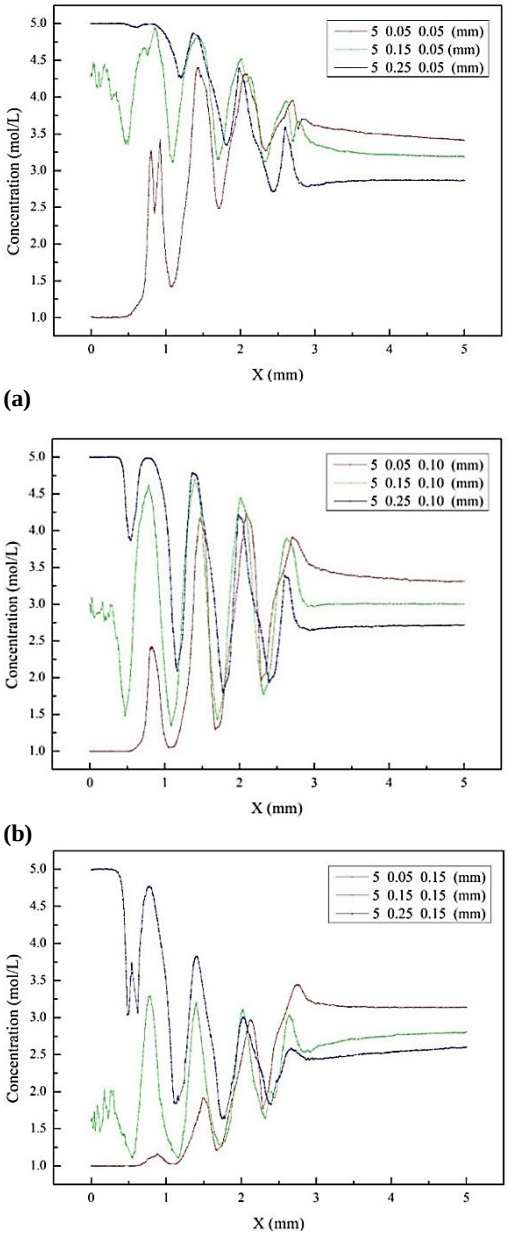

Fig. 15. Micromixer concentration curve along the X-axis direction with locations represented (y = 0.05, 0.15, 0.25 and a) z 0.05, b) z 0.10, c) z 0.15) at Re 5.

The effect of TSFM on the concentration distribution was analysed through the micromixer concentration curve along the X direction as shown in Figs. 14-16. The concentration data were collected using the y-z coordinate system with three parts coordinates namely green, red, and blue. The distances on the y-axis are 0.15 mm, 0.05 mm, and 0.25 mm. The three parts coordinates are 0.10 mm, 0.05 mm, and 0.15 mm on their respective z-axis distances.

Figure 14 shows the concentration curve on the X-axis, which varies significantly but the fluctuation is relatively small. When the z-axis is 0.10 mm, 0.05 mm or 0.15 mm in height, three sections of the concentration curve converge at 3 mol/L at the outlet.

Figure 15 shows the concentration curve at Re 5 fluctuating more sharply. As a result of the deflection phenomena, the fluid direction in the microchannel changes. At Re 5 the fluid residence time in the microchannels is short and the deflection phenomenon cannot produce strong eddies. This causes the three curves are not mix thoroughly at a concentration of 3 mol/L.

Figure 16 illustrates the convergence curve at various points at Re 100. At Re 100, the vortex is created as the liquid flows through the microchannel and enhances chaotic convection. When the liquid flows outside of the mixed region, the concentration curve is wholly mixed at a concentration of 3 mol/L and reaches a perfect mixing efficiency. Hence, from the

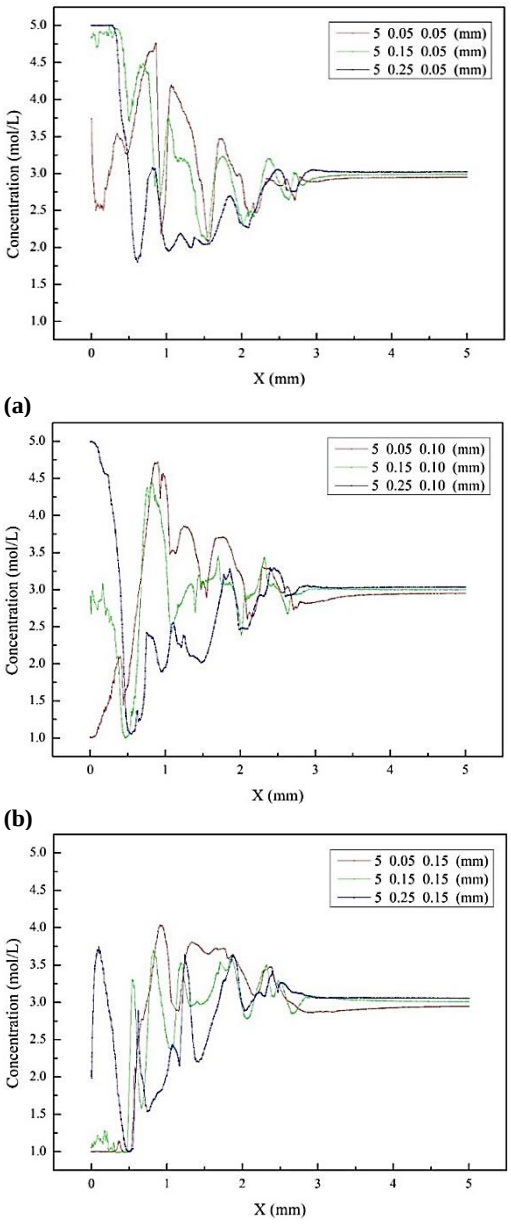

Fig. 16. Micromixer concentration curve along the X-axis direction with locations represented (y = 0.05, 0.15, 0.25 and a) z 0.05, b) z 0.10, c) z 0.15) at Re 100.

convergence of the concentration curve throughout the microchannel direction, it was shown that the phenomena of deflection caused by TSFM significantly drive the increase in mixing efficiency.

In this paper, the pressure drop effect is also studied. Pressure drop occurs due to friction between fluids or through walls. This cannot be ignored because it can cause a cavitation effect, and the energy required for the liquid to flow also increases. Fig. 17 shows a visualisation of the pressure drop at each Re for the TSFM structure.

Based on Figure 17, it is found that the pressure drops from high to low, at Re 100, 5, and 0.05, respectively. A significant pressure drop is caused by a higher flow velocity and a slight pressure drop due

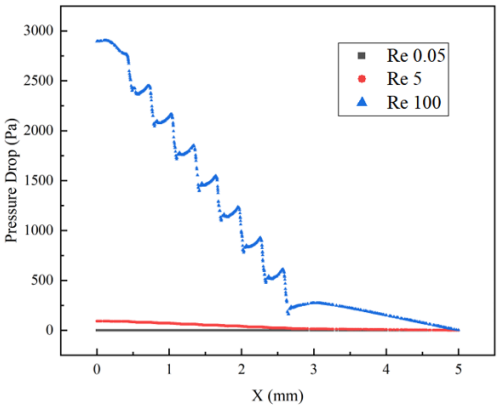

Fig. 17. Pressure drop at Re 0.05, 5, and 100.

to a lower flow velocity (Lv *et al*. 2021). Pressure drop plays an essential role in cell culture, and a low decrease can contribute to increased cell activity. Therefore, the selection of the Re number is adjusted based on the critical needs.

Based on the results of the comparisons in various Re as shown in Table 2, the design of the Koch fractal structure and the mixing efficiency was improved. Therefore, the better mixing efficiency with a channel length of 5 mm is obtained.

Table 2 Comparison of Koch fractal structures in the literature

Structure	Dimension	Re	Mixing Efficiency
Koch fractal micromixer with rounding corners structure (Chen *et al*. (2019))	15.3 mm	0.1-100	>87.5%
Koch fractal baffles micromixer (Zhang *et al*. 2019)	5.3 mm	0.05 -100	>60%
Koch snowflakes fractal (in this study)	5 mm	0.05 -100	>92%

5. CONCLUSION

This paper focuses on the mixing performance of a micromixer with a Koch fractal resistance and a design that has two types of resistance namely SSFM and TSFM. The angle and inlet factors affecting the mixing efficiency were studied by COMSOL Multiphysics. This study shows that the TSFM structure with an angle of 30° at the T-vortex inlet gets the best mixing efficiency. However, Re 0.05 and 100 showed a mixing efficiency of <0.95, which indicate near to perfect mixing. Concentration simulations at three Re (0.05, 5, 100) revealed that two fluids with varying concentrations exhibit a deflection phenomenon thereby escalates the contact area between the fluids. At Re 100, the liquid produces a vortex which the contact area of the two

liquids turns is noticeable and very irregular. This phenomenon increases the turbulent convection of the liquid and promotes molecular diffusion. This study shows that the TSFM structure can significantly improve the mixing efficiency. The optimize design is expect can be applied to LoC applications that require high mixing efficiency and compact structure.

ACKNOWLEDGMENTS

The authors thank UPI to provide the facility for conducting progress meetings and IMEN, UKM to provide the software used in this study. This research was supported by funding from the Ministry of Education and Culture Indonesia with grant 275/UN40.LP/PT.01.03/2021 and Universitas Pendidikan Indonesia through World Class University (WCU) Program.

REFERENCES

Ansari, M. A., K. Y. Kim, K. Anwar and S. M. Kim (2012). Vortex Micro T-mixer with Non-Aligned Inputs. *Chemical Engineering Journal* 181, 846-850.

Bahrami, D., A. A. Nadooshan and M. Bayareh (2020). Numerical Study on the Effect of Planar Normal and Halbach Magnet Arrays on Micromixing. *International Journal of Chemical Reactor Engineering* 18(9).

Balasubramaniam, L., R. Arayanarakool, S. D. Marshall, B. Li, P. S. Lee and P. C. Chen (2017). Impact of Cross-Sectional Geometry on Mixing Performance of Spiral Microfluidic Channels Characterized by Swirling Strength of Dean-Vortices. *Journal of Micromechanics and Microengineering* 27(9), 095016.

Bayareh, M. (2021). Artificial Diffusion in the Simulation of Micromixers: a Review. *Journal of Mechanical Engineering Science* 235(21), 5288-5296.

Bayareh, M., A. Usefian and A. A. Nadooshan (2019). Rapid Mixing of Newtonian and non-Newtonian Fluids in a Three-Dimensional Micromixer Using Non-Uniform Magnetic Field. *Journal of Heat and Mass Transfer Research* 6(1), 55-61.

Bayareh, M., M. N. Ashani and A. Usefian (2020). Active and Passive Micromixers: A Comprehensive Review. *Chemical Engineering and Processing-Process Intensification* 147, 107771.

Bazaz, S. R., A. A. Mejrizi and S. M. Javid (2016). *Canadian Society for Mechanical Engineering (CSME) International Conference*, Canada, June

Borgohain P., J. Arumughan, A. Dalal and G. Natarajan (2018). Design and Performance of a Three-Dimensional Micromixer with Curved Ribs *Chemical engineering research and design* 136, 761–775.

Cai, G., L. Xue, H. Zhang and J. Lin (2017). A Review on Micromixers. *Micromachines* 8(9), 274.

Chen, X. and S. Zhang (2018). 3D Micromixers Based on Koch Fractal Principle. *Microsystem Technologies* 24(6), 2627-2636.

Chen, X. and T. Li (2017). A Novel Passive Micromixer Designed by Applying an Optimization Algorithm to the Zigzag Microchannel. *Chemical Engineering Journal* 313, 1406-1414.

Chen, X. and Z. Zhao (2017). Numerical Investigation on Layout Optimization of Obstacles in A Three-Dimensional Passive Micromixer. *Analytica chimica acta* 964, 142-149.

Chen, X., S. Liu, Y. Chen and S. Wang (2021). A Review on Species Mixing in Droplets Using Passive and Active Micromixers. *International Journal of Environmental Analytical Chemistry* 101(3), 422-432.

Chen, X., S. Zhang, Z. Wu and Y. Zheng (2019). A Novel Koch Fractal Micromixer with Rounding Corners Structure. *Microsystem Technologies* 25(7), 2751-2758.

Chen, Y. and C. N. Kim (2018). Numerical Analysis of the Mixing of Two Electrolyte Solutions in an Electromagnetic Rectangular Micromixer. *Journal of industrial and engineering chemistry* 60, 377-389.

Chen, Y., X. Chen and S. Liu (2020). Numerical and Experimental Investigations of Novel Passive Micromixers with Fractal-Like Tree Structures. *Chemical Physics Letters* 747, 137330.

Fatimah, N., B. Mulyanti, R. E. Pawinanto and A. B. Pantjawati (2020). *2020 3rd International Conference on Computer and Informatics Engineering (IC2IE)*, Yogyakarta, Indonesia, December

Hama, B., G. Mahajan, P. S. Fodor, M. Kaufman and C. R. Kothapalli (2018). Evolution of Mixing in a Microfluidic Reverse-Staggered Herringbone Micromixer. *Microfluidics and Nanofluidics* 22(5), 1-14.

Huang, C. Y., Y. H. Hu, S. A. Wan and H. Nagai (2020). Application of Pressure-Sensitive Paint for The Characterization of Mixing with Various Gases in T-Type Micromixers. *International Journal of Heat and Mass Transfer* 156, 119710.

Keçili, R., F. Ghorbani-Bidkorbeh, I. Dolak, İ and C. M. Hussain (2020). *Era of Nano-Lab-on-a-Chip (LOC)*. Elsevier, 1-17.

Liu, G., X. Ma, C. Wang, X. Sun and C. Tang (2018). Piezoelectric Driven Self-Circulation Micromixer with High-Frequency Vibration. *Journal of Micromechanics and Microengineering* 28(8), 085010.

Lv, H. and X. Chen (2021). New insights into the

mechanism of fluid mixing in the micromixer based on alternating current electric heating with film heaters. International Journal of Heat and Mass Transfer 181, 121902.

Lv, H., X. Chen and X. Zeng (2021). Optimization of micromixer with Cantor fractal baffle based on simulated annealing algorithm. Chaos, Solitons & Fractals 148, 111048.

Mehrdel, P., S. Karimi, J. Farré-Lladós, and J. Casals-Terré (2018). Novel Variable Radius Spiral–Shaped Micromixer: From Numerical Analysis to Experimental Validation. *Micromachines* 9(11), 552.

Mondal, B., S. K. Mehta, P. K. Patowari and S. Pati (2019). Numerical Study of Mixing in Wavy Micromixers: Comparison Between Raccoon and Serpentine Mixer. *Chemical Engineering and Processing-Process Intensification* 136, 44-61.

Pawinanto, R. E., J. Yunas and A. M. Hashim (2020). Micropillar Based Active Microfluidic Mixer for The Detection of Glucose Concentration. *Microelectronic Engineering* 234, 111452.

Rafeie, M., M. Welleweerd, A. Hassanzadeh-Barforoushi, M. Asadnia, W. Olthuis and M. E. Warkiani (2017). An Easily Fabricated Three-Dimensional Threaded Lemniscate-Shaped Micromixer for a Wide Range of Flow Rates. *Biomicrofluidics* 11, 1.

Raza, W. and K. Y. Kim (2020). Unbalanced Split and Recombine Micromixer with Three-Dimensional Steps. *Industrial & Engineering Chemistry Research* 59(9), 3744-3756.

Rohman, A. S., B. Mulyanti, R. E. Pawinanto and A. B. Pantjawati (2020). *2020 3rd International Conference on Computer and Informatics Engineering (IC2IE)*, Yogyakarta, Indonesia, December

Sarma, P. and P. K. Patowari (2016). Design and Analysis of Passive Y-Type Micromixers for Enhanced Mixing Performance for Biomedical and Microreactor Application. *Journal of Advanced Manufacturing Systems* 15(03), 161-172.

Shi, X., L. Wang, S. Huang and F. Li (2021). A Novel Passive Micromixer with Array of Koch Fractal Obstacles in Microchannel. *Journal of Dispersion Science and Technology* 42(2), 236-247.

Thiermann, R., R. Bleul and M. Maskos (2017). Kinetic Control of Block Copolymer Self‐Assembly in a Micromixing Device—Mechanistical Insight into Vesicle Formation Process. *Macromolecular Chemistry and Physics* 218(2), 1600347.

Usefian, A.and M. Bayareh (2019). Numerical and Experimental Study on Mixing Performance of a Novel Electro-Osmotic Micro-Mixer. *Meccanica* 54(8) 1149–1162.

Wu, Z. and X. Chen (2019). A Novel Design for Passive Micromixer Based on Cantor Fractal Structure. *Microsystem Technologies* 25(3), 985-996.

Zhang, S., X. Chen, Z. Wu and Y. Zheng (2019). Numerical Study on Stagger Koch Fractal Baffles Micromixer. *International Journal of Heat and Mass Transfer* 133, 1065-1073.